Hindawi
International Journal of Aerospace Engineering
Volume 2022, Article ID 5191568, 17 pages
https://doi.org/10.1155/2022/5191568

Research Article

Prescribed Performance Guidance Law with Multiple Constraints

Xu Li, Jikun Ye, Chijun Zhou, and Xiao Tang

Air and Missile Defense College, Air Force Engineering University, Shanxi, Xi'an 710051, China

Correspondence should be addressed to Jikun Ye; jikunbo@sina.com

Received 21 March 2022; Revised 13 May 2022; Accepted 4 June 2022; Published 27 June 2022

Academic Editor: Paolo Castaldi

In the terminal guidance phase of intercepting aerial target, a guidance law, satisfying impact angle constraint, acceleration constraint, and second-order dynamic characteristic of interceptor autopilot, is designed based on the prescribed performance control and dynamic surface control method. Firstly, a two-dimensional plane interception model considering the dynamic characteristics of autopilot and input constraints is established. Furthermore, for the nonconstrained system, based on the dynamic surface control, the prescribed performance reaching law is used to ensure that the line-of-sight angle and the line-of-sight angle rate can converge to the prescribed range in finite time. At the same time, an adaptive law is used to estimate the uncertainty caused by target maneuver and autopilot. Then, aiming at the acceleration constraint, an auxiliary system is established to convert the restricted system into a nonrestricted system. The finite-time convergence of the terminal line-of-sight tracking error, the line-of-sight rate, and the uniform ultimate boundedness of the system are rigorously proved by Lyapunov stability theory. Finally, the simulation results show that the proposed guidance law can make the interceptor have better interception performance when attacking targets with different maneuvering forms.

1. Introduction

In the terminal guidance phase of high-speed maneuvering target interception, the final miss distance between the missile and the maneuvering target is often used as an important indicator of the guidance law design. In addition, direct collision is the most effective way to intercept high-speed maneuvering target, which requires the interceptor to attack the target at a specific impact angle to improve the success rate of direct collision [1]. Therefore, it is necessary to design a guidance law to meet the impact angle constraint.

In the actual execution of the guidance law, there is a certain time delay between the guidance command signal and the control rudder deflection signal due to the dynamic characteristics of the missile's autopilot. It is difficult to ensure the guidance accuracy without considering the autopilot delay dynamics, especially for intercepting maneuvering targets [2].What is more, due to the limited capability of missile's actuator, the acceleration constraint should be concerned. A series of nonlinear guidance laws were designed for the guidance system with acceleration saturation constraint, but only for stationary targets [3–5]. At present, there are few studies on the guidance problem of maneuvering target, considering the second-order dynamic characteristics of missile's autopilot and the input limitation. For example, the dynamic surface guidance law is designed to meet the second-order dynamic characteristics of the missile's autopilot but did not consider the control input constraints in [6]. In [7], based on the differentiator, backstepping method, and adaptive technology, an adaptive guidance law is designed for impact angle constraint and second-order dynamic characteristics of autopilot which did not consider the input saturation, and the adaptive parameters were not bounded in the guidance process.

In order to design guidance law with constraints, experts and scholars have conducted a lot of research based on sliding mode control (SMC) methods and have obtained many valuable results [8–11]. Since the sliding mode control has the characteristics of robustness and easy realization for the system uncertainty, many guidance laws with terminal

line-of-sight angle constraint are designed based on sliding mode control theory. In reference [12], a nonsingular terminal sliding mode guidance law is designed satisfying impact angle constraint based on nonsingular sliding mode control theory; in reference [13], an adaptive sliding mode guidance law is designed based on adaptive control technology and nonlinear sliding mode control theory, satisfying the first order dynamic delay of autopilot; in reference [14], an adaptive dynamic surface guidance law is designed by using barrier Lyapunov function under the view constraint of seeker and first order dynamic characteristics of autopilot; in reference [15], a sliding mode guidance law is designed, considering the autopilot as a first-order dynamic characteristic, using online homogeneous observer to estimate the line-of-sight (LOS) angular rate; in reference [16], a sliding mode dynamic surface guidance law is designed for the case of impact angle constraint and missile second-order autopilot's dynamics.

The guidance law design based on SMC includes two parts: the design of sliding mode surface and the design of reaching law. The sliding mode surface is designed to ensure that each item constituting the sliding mode surface can converge to the predetermined value, such as the system state and tracking error. The forms of sliding mode surface are diverse, and the commonly used sliding mode is linear sliding mode, nonsingular terminal sliding mode, integral sliding mode, and fractional sliding mode [17]. The sliding mode reaching law mainly includes constant velocity reaching law, exponential reaching law, and general reaching law [18]. The reaching law can make the sliding mode variable converge quickly and then guarantee that the system state or tracking error reaches the sliding mode surface.

In the design of the sliding mode guidance law, the convergence performance of the sliding mode variable can be achieved by adjusting the parameters of the reaching law. However, the reaching law designed based on the Lyapunov theory and the finite-time convergence theory cannot guarantee the same convergence effect under different interception conditions. It is not easy to find the appropriate parameters to ensure the transient convergence performance of the sliding mode variable, especially at the beginning of the terminal guidance.

In recent years, prescribed performance control (PPC) has been widely used in the design of guidance and control systems [19–21]. In reference [22], the attitude tracking error of spacecraft is limited to the prescribed range by using the prescribed performance method. In reference [23], the prescribed performance method for hypersonic vehicle height control is proposed to ensure the desired dynamic performance and steady-state accuracy.

Based on the PPC theory, the tracking error can converge according to the convergence range predefined by the prescribed performance function (PPF), which provides a simple method for the transient and steady-state performance of error convergence.

In order to solve the input constraint, impact angle constraint, and missile's autopilot delay constraint, an adaptive prescribed performance guidance law is designed by introducing auxiliary system, adaptive technology, low-pass filter, backstepping method, and prescribed performance control technology. An improved PPF is applied to design guidance law with constraints, ensuring the sliding mode variable convergence to the predefined range. Finally, the effectiveness is verified by digital simulation.

2. Problem Description

The relative motion of two-dimensional pitching plane is shown in Figure 1. The relative motion equation is as follows:

$$\dot{R} = V_T \cos \eta_T - V_M \cos \eta_M, \tag{1}$$

$$R\dot{q} = -V_T \sin \eta_T + V_M \sin \eta_M, \tag{2}$$

$$\dot{\theta}_M = \frac{a_M}{V_M}, \tag{3}$$

$$\dot{\theta}_T = \frac{a_T}{V_T}, \tag{4}$$

where $\theta_M = q - \eta_M$; $\theta_T = q - \eta_T$; R is the relative distance between the missile and the target; $\dot{R}$ is the relative velocity between the missile and the target; V_M and V_T, respectively, represent the velocity of the missile and the target; θ_M and θ_T, respectively, represent the trajectory inclination angle of the missile and the flight path angle of the target; q and $\dot{q}$, respectively, represent the LOS angle and the LOS angular rate of the missile and the target; a_M and a_T, respectively, represent the normal acceleration acting on the missile and the target. Kinematic trajectory of missile can be obtained by integrating relative motion equations.

Although the actual missile autopilot has high-order dynamic characteristics, it can be approximated as the following form of second-order dynamic characteristics in the design of guidance law.

$$\ddot{u}_q = -2\zeta\omega_n \dot{u}_q - \omega_n^2 u_q + \omega_n^2 u_\theta + d_2, \tag{5}$$

where ζ represents the damping ratio, ω_n represents the natural frequency, u_q represents the actual guidance command, u_θ represents the ideal guidance command, and d_2 is the uncertainty of the model. Considering the input constraint condition, equation (5) can be rewritten as follows:

$$\ddot{u}_q = -2\zeta\omega_n \dot{u}_q - \omega_n^2 u_q + \omega_n^2 \mathrm{sat}(u_\theta) + d_2, \tag{6}$$

where $\mathrm{sat}(\cdot)$ represents the saturation function which satisfy the following requirements

$$\mathrm{sat}(u_\theta) = \begin{cases} u_{\max}, u_\theta > u_{\max}, \\ u_\theta, -u_{\max} \le u_\theta \le u_{\max}, \\ -u_{\max}, u_\theta < u_{\max}, \end{cases} \tag{7}$$

where $u_{\max}$ denotes the upper bound of the known guidance command. Synthesizing equations (1)–(7), the plane guidance equation with impact angle constraint, input constraint, and

autopilot second-order dynamic characteristics is

$$\begin{cases} \dot{x}_1 = x_2, \\ \dot{x}_2 = -\dfrac{2\dot{R}}{R}x_2 - \dot{\psi}_l^2 \sin x_1 \cos x_1 - \dfrac{1}{R}x_3 + d_1, \\ \dot{x}_3 = x_4, \\ \dot{x}_4 = -2\zeta\omega_n x_4 - \omega_n^2 x_3 + \omega_n^2 \mathrm{sat}(u_\theta) + d_2, \end{cases} \tag{8}$$

where $d_1 = a_T \cos \eta_T / R$ is the uncertainty of target maneuver, d_2 is the uncertainty of the autopilot, state variable $x_1 = q - q_d$, $x_2 = \dot{x}_1 = \dot{q}$, $x_3 = u_q$, $x_4 = \dot{u}_q$, and q_d is the expected LOS angle in the longitudinal plane. In the process of terminal guidance, we consider $\dot{R} \approx$ const so that $\ddot{R} \approx 0$.

The target designed in this paper: for the guidance model (8) with multiple constraints, a prescibed performance guidance law is designed based on adaptive dynamic surface method, and the corresponding stability proof is given. A low-pass filter is introduced to avoid the phenomenon of "differential expansion" caused by multiple derivative of virtual control. At the same time, a new adaptive algorithm is used to estimate the unknown upper bound of external interference online. Finally, the effectiveness of the guidance law is verified by digital simulation.

3. Basic Theory of Prescibed Performance Control

3.1. Performance Function. By introducing the performance function, the transient and steady-state performances of tracking error $e(t)$ are set, and the performance function is defined as follows.

Definition 1. The continuous function $\rho : R_+ \longrightarrow R_+$ is called the performance function, which satisfies:

(1) $\rho(t)$ is positive and strictly decreasing

(2) $\lim_{t\longrightarrow\infty} \rho(t) = \rho_\infty > 0$

On the premise that the initial error $e(0)$ is known, the inequality constraints are given:

$$\begin{cases} -\delta\rho(t) < e(t) < \rho(t), & e(0) > 0, \\ -\rho(t) < e(t) < \delta\rho(t), & e(0) < 0, \end{cases} \tag{9}$$

where $t \in [0,\infty)$, $\delta \in [0, 1]$.

This paper selects the form of performance function as follows:

$$\rho(t) = (\rho_0 - \rho_\infty) \exp(-lt) + \rho_\infty. \tag{10}$$

where l is the convergence coefficient and ρ_0 is the initial value of $\rho(t)$. If inequality (9) holds, the error curve will be limited between $-\delta\rho(t)$ and $\rho(t)$. In addition, combined with the decreasing characteristics of $\rho(t)$, it can be seen that the error $e(t)$ will rapidly converge to a neighborhood of 0

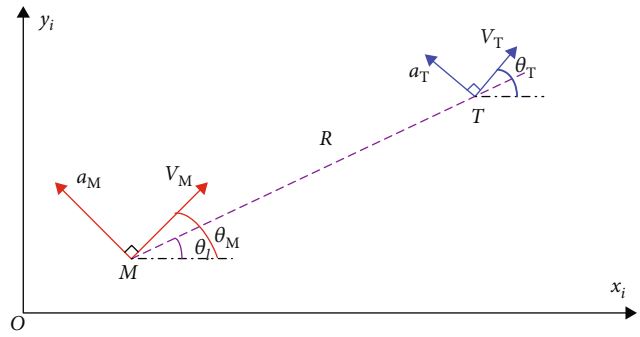

Figure 1: Missile-target relative motion relations.

under the clamping force of $-\delta\rho(t)$ and $\rho(t)$. Constant ρ_∞ is the upper bound of the preset steady-state error, the decay rate of $\rho(t)$ is the lower bound of the convergence rate of the tracking error $e(t)$, and the maximum overshoot of the tracking error is not greater than $\delta\rho(0)$. Therefore, the steady and transient state of the tracking error can be restricted by selecting the appropriate performance function $\rho(t)$ and constant δ.

3.2. Error Transformation. In the process of system design, it is very difficult to deal with inequality constraints directly. The error transformation function $S(\varepsilon)$ is used to transform inequality constraints into equality constraints and then deal with them. The error transformation function is defined as follows:

$$S(\varepsilon) = \frac{\iota_{\mathrm{up}} \exp(\varepsilon) - \iota_{\mathrm{down}} \exp(-\varepsilon)}{\exp(\varepsilon) + \exp(-\varepsilon)}, \tag{11}$$

where ι_{up}, ι_{down} is the normal number of the design. Equation (11) satisfies

$$\begin{cases} -\iota_{\mathrm{down}} < S(\varepsilon) < \iota_{\mathrm{up}}, \\ \lim_{\varepsilon\longrightarrow-\infty} S(\varepsilon) = -\iota_{\mathrm{down}}, \\ \lim_{\varepsilon\longrightarrow+\infty} S(\varepsilon) = \iota_{\mathrm{up}}. \end{cases} \tag{12}$$

Besides, for $\forall\varepsilon \in (-\infty, +\infty)$, $dS(\varepsilon)/d\varepsilon > 0$ are bounded, and $S(\varepsilon)$ is sufficiently smooth and strictly monotone increasing bounded.

The relationship between tracking error e and transformation error ε can be expressed as

$$e(t) = \rho(t)S(\varepsilon). \tag{13}$$

The error transformation function $S(\varepsilon)$ is simplified as

$$S(\varepsilon) = \iota_{\mathrm{up}} - \frac{\iota_{\mathrm{up}} + \iota_{\mathrm{down}}}{\exp(2\varepsilon) + 1}. \tag{14}$$

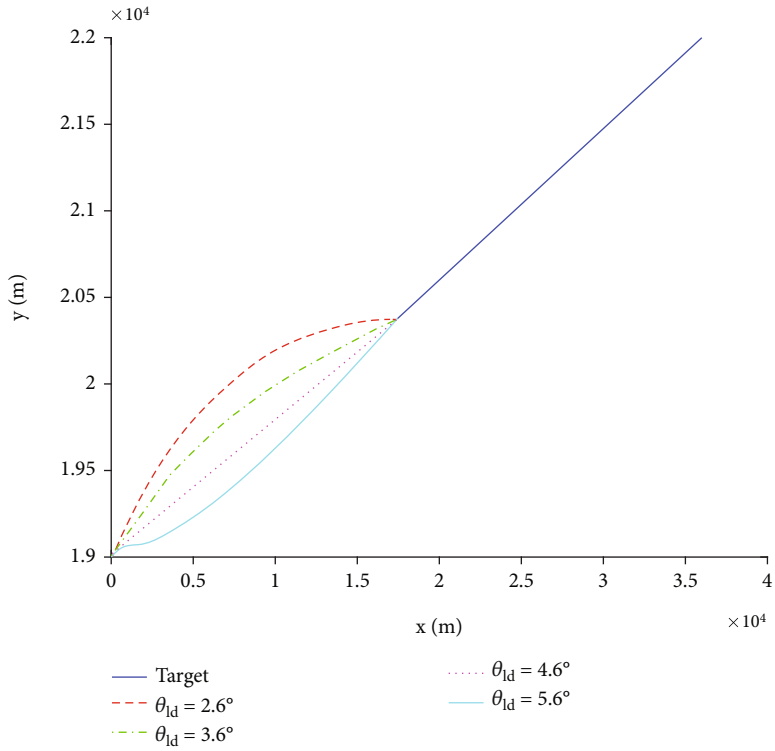

Figure 2: Trajectory curve.

The inverse function of $S(\varepsilon)$ can be obtained:

$$\varepsilon = \frac{1}{2} \ln \left(\frac{\iota_{up} + \iota_{down}}{\iota_{up} - S(\varepsilon)} - 1 \right). \tag{15}$$

Let $T = S^{-1}$ denote the inverse function of function S, then formula (15) can be equivalently expressed as

$$\varepsilon = T\left(\frac{e}{\rho}\right). \tag{16}$$

If $\varepsilon(t) \in \ell_\infty$ and $t \in [0,\infty)$, then the inequality constraint (9) is satisfied. With the convergence of $\rho(t)$, the tracking error will eventually be limited in the following range:

$$E = \left\{ e \in R : -\iota_{down}\rho_\infty < e(t) < \iota_{up}\rho_\infty \right\}. \tag{17}$$

4. Design of Prescribed Performance Guidance Law

For guidance system (8), the prescribed performance adaptive dynamic surface guidance law is designed, and the corresponding stability analysis is given. By introducing a low-pass filter, the "differential expansion" phenomenon caused by multiple derivations of virtual control is avoided. The unknown upper bounds of external disturbances d_1 and d_2 are estimated online by using a new adaptive algorithm, which can ensure that the adaptive parameters are bounded in the guidance process. The specific process is as follows.

Step 1. Firstly, the guidance law is designed in the two-dimensional plane, and the linear sliding mode surface is constructed according to the line-of-sight angle error x_1 and line-of-sight angle rate x_2 in the pitch plane.

$$s_1 = c_1 x_1 + c_2 x_2. \tag{18}$$

The constants c_1 and c_2 are positive and satisfy Hurwitz stability. When $s_1 = 0$ holds, x_1 and x_2 approach 0 in finite time.

Set the tracking error to be $z_1 = s_1 - 0$, the derivation of tracking error is calculated as

$$\dot{z}_1 = c_1 \dot{x}_1 + c_2 \dot{x}_2. \tag{19}$$

Using error conversion function:

$$\begin{aligned} S_1(\varepsilon_1) &= \frac{\iota_{up,1} \exp(\varepsilon_1) - \iota_{down,1} \exp(-\varepsilon_1)}{\exp(\varepsilon_1) + \exp(-\varepsilon_1)}, \\ \rho_1(t) &= \left(\rho_{0,1} - \rho_{\infty,1}\right) \exp(-l_1 t) + \rho_{\infty,1}, \end{aligned} \tag{20}$$

where $\iota_{up,1}, \iota_{down,1}$ is the normal number of design, ρ_1 is the performance function, $\rho_{0,1}$ and $\rho_{\infty,1}$ are the boundary value, and $T_1 = S_1^{-1}$ is the inverse function of S_1. Then, the transformation error can be expressed as

$$\varepsilon_1 = T_1\left(\frac{z_1}{\rho_1}\right). \tag{21}$$

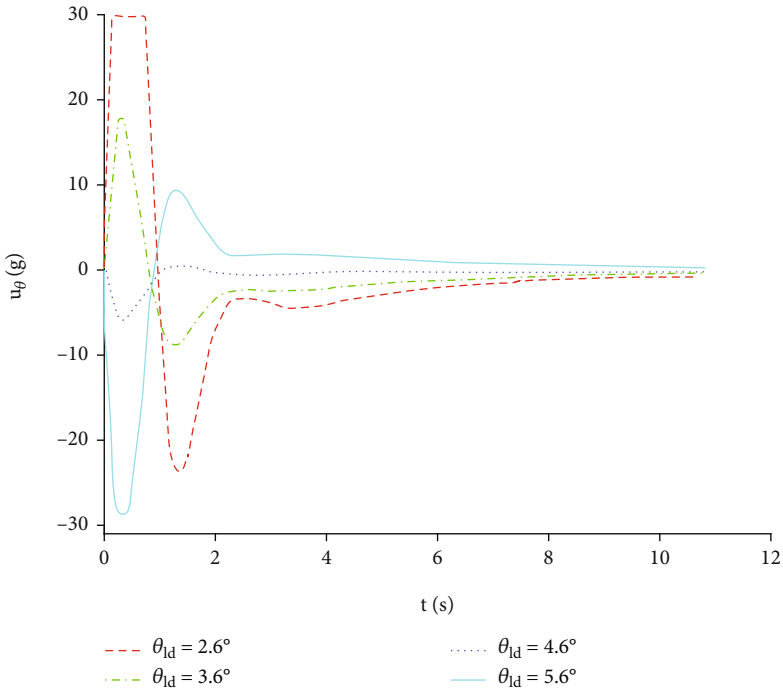

Figure 3: Missile acceleration curve.

The derivative of (21) is

$$\dot{\varepsilon}_1 = \frac{dT_1}{d(z_1/\rho_1)}\frac{\dot{z}_1}{\rho_1} - \frac{dT_1}{d(z_1/\rho_1)}\frac{\dot{\rho}}{{\rho_1}^2}z_1. \tag{22}$$

Combining the guidance model (8) with the transformed error rate equation (23), it can be obtained:

$$\begin{cases} \dot{\varepsilon}_1 = \dfrac{dT_1}{d(z_1/\rho_1)}\dfrac{\dot{z}_1}{\rho_1} - \dfrac{dT_1}{d(z_1/\rho_1)}\dfrac{\dot{\rho}_1}{{\rho_1}^2}z_1, \\ \dot{z}_1 = c_1\dot{x}_1 + c_2\dot{x}_2, \\ \dot{x}_2 = -\dfrac{2\dot{R}}{R}x_2 - \dot{\psi}_l^2 \sin x_1 \cos x_1 - \dfrac{1}{R}x_3 + d_1. \end{cases} \tag{23}$$

Therefore, $\dot{\varepsilon}_1$ can also be expressed as

$$\dot{\varepsilon}_1 = \frac{r_1}{\rho_1}\left(c_1x_2 + c_2\left(-\frac{2\dot{R}}{R}x_2 - \dot{\psi}_l^2 \sin x_1 \cos x_1 - \frac{1}{R}x_3 + d_1\right)\right) - r_1\frac{\dot{\rho}_1}{{\rho_1}^2}z_1, \tag{24}$$

where $r_1 = dT_1/d(z_1/\rho_1) > 0, \rho_1 > 0$. Introducing a virtual control law x_{3c} to ensure that $\varepsilon_1 \longrightarrow 0$. x_{3c} is designed as

$$x_{3c} = -R\dot{\psi}_l^2 \sin x_1 \cos x_1 - 2\dot{R}x_2 - \frac{R}{c_2}x_2 - R\frac{\dot{\rho}_1}{\rho_1}z_1 + R\frac{\rho_1}{r_1}k_1\varepsilon_1 + R\hat{d}_1, \tag{25}$$

where k_1 is a positive constant and $\hat{d}_1$ is the estimated value of the disturbance term d_1. Assuming that the actual disturbance d_1 changes slowly, it can be concluded that $\dot{d}_1 \approx 0$. The following adaptive law is designed to estimate d_1

$$\dot{\hat{d}}_1 = -\sigma_1\hat{d}_1 - \frac{r_1}{\rho_1}c_2\varepsilon_1, \tag{26}$$

where σ_1 is adaptation coefficient. Selecting Lyapunov function as

$$V_{\varepsilon_1} = \frac{1}{2}\varepsilon_1^2 + \frac{1}{2}\tilde{d}_1^2, \tag{27}$$

where $\tilde{d}_1$ is the estimation error

$$\tilde{d}_1 = d_1 - \hat{d}_1. \tag{28}$$

Combining (27) and (28), the derivative of (27) is calculated as

$$\dot{V}_{\varepsilon_1} = \varepsilon_1\dot{\varepsilon}_1 = -c_2\frac{r_1}{\rho_1}\frac{1}{R}y_2\varepsilon_1 - c_2k_1\varepsilon_1\varepsilon_1 + \sigma_1\hat{d}_1\tilde{d}_1, \tag{29}$$

where y_2 is the filtering estimation error, which is defined in the next section. A low-pass filter is designed to avoid differential expansion caused by derivative of virtual control

$$\tau_1\dot{x}_{3d} + x_{3d} = x_{3c}, x_{3d}(0) = x_{3c}(0). \tag{30}$$

Among them, τ_1 is the filter time constant.

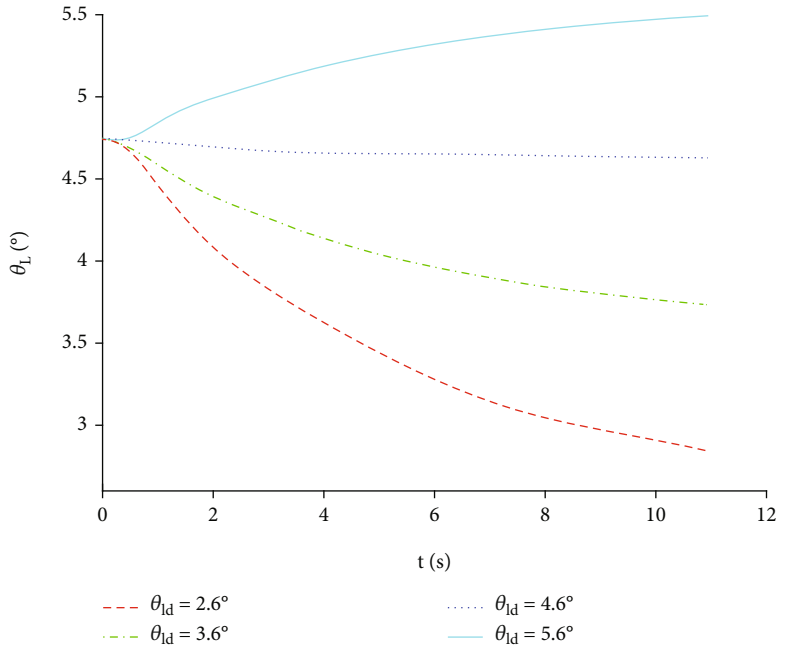

Figure 4: Change curve of LOS angular.

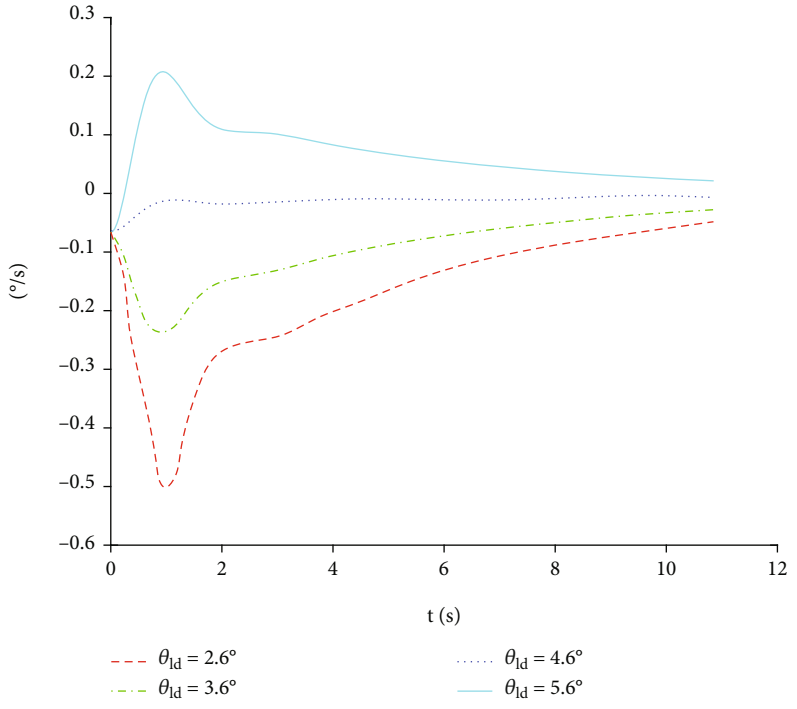

Figure 5: Change curve of LOS angular rate.

Step 2. Define z_2 as tracking error between virtual control x_{3c} and actual state x_3

$$z_2 = x_3 - x_{3c}. \tag{31}$$

The derivation of tracking error (31) is calculated as

$$\dot{z}_2 = x_4 - \dot{x}_{3d}. \tag{32}$$

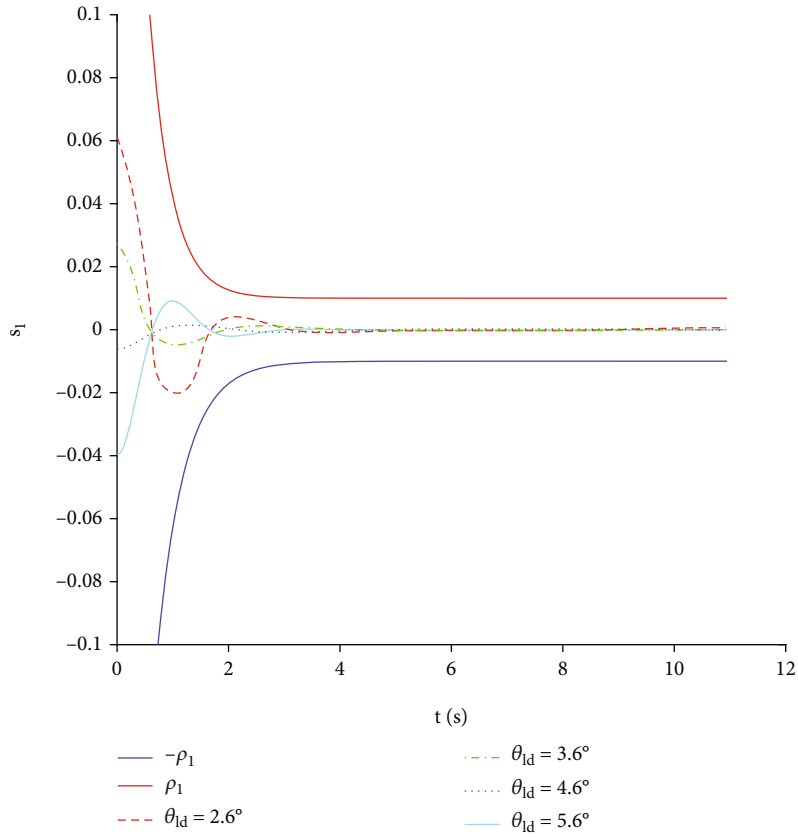

Figure 6: Change curve of sliding surface.

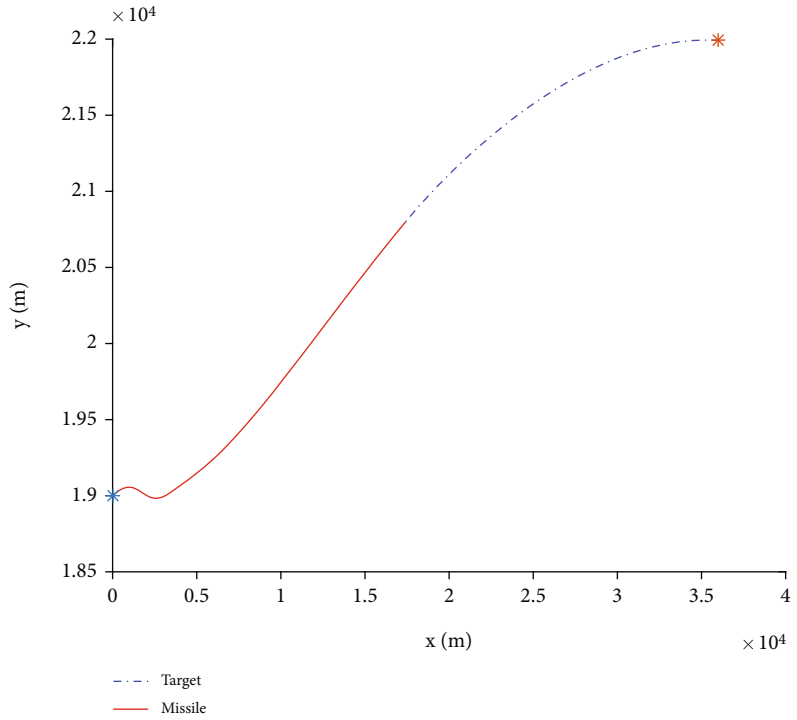

Figure 7: Trajectory curve.

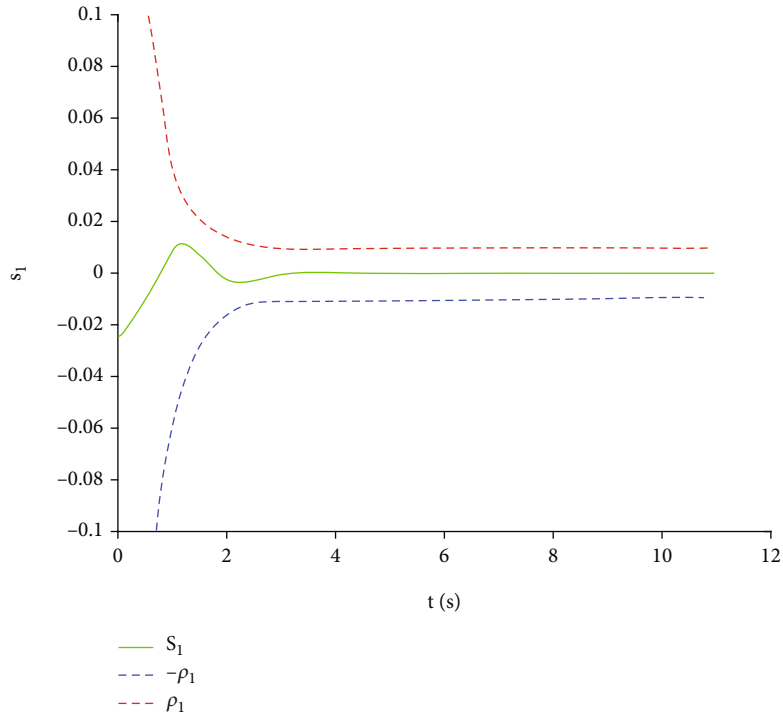

Figure 8: Change curve of sliding surface.

Virtual control law x_{4c} is

$$x_{4c} = -k_2 z_2 + \dot{x}_{3d} + \frac{c_2 r_1}{R\rho_1}\varepsilon_1, \tag{33}$$

where k_2 is a positive constant. And define a Lyapunov function as

$$V_{z_2} = \frac{1}{2}z_2^2. \tag{34}$$

The derivation of V_{z_2} is calculated as

$$\dot{V}_{z_2} = z_2\dot{z}_2 = z_2(z_3 + x_{4c} + y_3 - \dot{x}_{3d}) = -k_2 z_2 z_2 + z_2 y_3, \tag{35}$$

where y_3 is the filtering estimation error, which is defined in the next section. A low-pass filter is designed to avoid differential expansion caused by derivative of virtual control

$$\tau_2\dot{x}_{4d} + x_{4d} = x_{4c}, x_{4d}(0) = x_{4c}(0). \tag{36}$$

Among them, τ_2 is the filter time constant.

Step 3. In order to eliminate the deviation caused by the acceleration constraint, an auxiliary system is introduced to compensate the acceleration error.

$$\dot{\chi}_{u_\theta} = -k_{u_\theta}\chi_{u_\theta} + \omega_n^2(\mathrm{sat}(u_\theta) - u_\theta), \tag{37}$$

where $k_{u_\theta} > 0$ is the parameter to be designed and χ_{u_θ} is the compensation quantity; the corrected state tracking error is redefined as

$$z_3 = x_4 - x_{4d} - \chi_{u_\theta}. \tag{38}$$

The derivation of (38) is calculated as

$$\dot{z}_3 = -2\zeta\omega_n x_4 - \omega_n^2 x_3 + \omega_n^2\mathrm{sat}(u_\theta) + d_2 - \dot{x}_{4d} + k_{u_\theta}\chi_{u_\theta} - \omega_n^2(\mathrm{sat}(u_\theta) - u_\theta). \tag{39}$$

So that the expected acceleration instruction u_θ can design as

$$u_\theta = \frac{1}{\omega_n^2}\left[-k_3 z_3 - z_2 + 2\zeta\omega_n x_4 + \omega_n^2 x_3 - \hat{d}_2 + \dot{x}_{4d} - k_{u_\theta}\chi_{u_\theta}\right], \tag{40}$$

where k_3 is a positive constant, $\hat{d}_2$ is the estimated value of the disturbance term d_2, and the actual disturbance d_2 changes slowly. Assuming that the actual disturbance d_2 changes slowly, we can obtain that $\dot{d}_2 \approx 0$. The adaptive

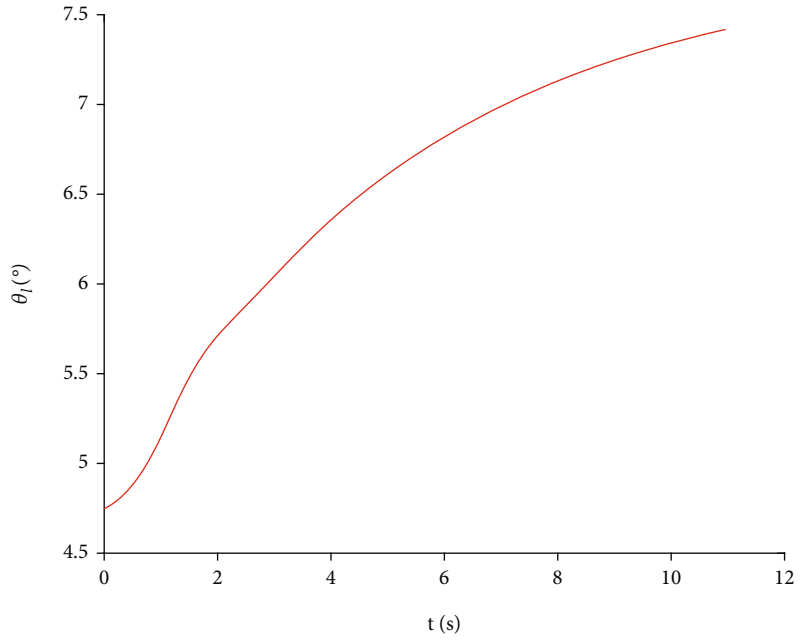

Figure 9: Change curve of LOS angular.

law is designed as

$$\dot{\hat{d}}_2 = -\sigma_2 \hat{d}_2 - z_3, \tag{41}$$

where σ_2 is the adaptation coefficient. Constructing Lyapunov function

$$V_{z_3} = \frac{1}{2} z_3^2 + \frac{1}{2} \tilde{d}_2^2. \tag{42}$$

Combining (39)–(42), the derivative of (42) is calculated as

$$\dot{V}_{z_3} = z_3 \dot{z}_3 + \tilde{d}\dot{\tilde{d}} = -k_3 z_3^2 + \sigma_2 \hat{d}_2 \tilde{d}_2. \tag{43}$$

5. Stability Proof of Guidance Law

Theorem 2. *For the pitch plane guidance subsystem (8) considering the impact angle constraint, the second-order dynamic characteristics of autopilot, and the acceleration constraint, it can ensure that the LOS rate converges in finite time and the LOS angle converges to the desired terminal LOS angle in finite time under the action of adaptive prescribed performance guidance law as shown in equation (40).*

Proof. Define filter estimation error:

$$y_i = x_{id} - x_{ic}, \quad i = 2, 3. \tag{44}$$

Constructing Lyapunov function:

$$V_{iy} = \frac{1}{2} y_i^2 i = 2, 3. \tag{45}$$

The derivative of (45) is calculated as

$$\dot{V}_{iy} = y_i \left(-\frac{y_i}{\tau_i} + \eta_i \right) = -\frac{2y_i^2}{\tau_i} + y_i \eta_i, \tag{46}$$

where $|\dot{x}_{ic}| \le \eta_i$ and η_i is a bounded normal number [24]. Constructing Lyapunov function

$$V = V_{\varepsilon 1} + V_{z2} + V_{z3} + V_{2y} + V_{3y}. \tag{47}$$

Calculate the derivative of V and combine (29), (35), (43), and (46), we can obtain that

$$\begin{aligned} \dot{V} &= \dot{V}_{\varepsilon 1} + \dot{V}_{z2} + \dot{V}_{z3} + \dot{V}_{2y} + \dot{V}_{3y} \\ &= -c_2 k_1 \varepsilon_1^2 - k_2 z_2^2 - k_3 z_3^2 - c_2 \frac{r_1}{\rho_1} \frac{1}{R} y_2 \varepsilon_1 + z_2 y_3 \\ &\quad + \sigma_1 \hat{d}_1 \tilde{d}_1 + \sigma_2 \hat{d}_2 \tilde{d}_2 - \frac{2y_2^2}{\tau_2} + y_2 \eta_2 - \frac{2y_3^2}{\tau_3} + y_3 \eta_3. \end{aligned} \tag{48}$$

In view of

$$\begin{cases} \hat{d}_1 \tilde{d}_1 = -\frac{1}{2} \left(\tilde{d}_1^2 - {d_1}^2 + \hat{d}_1^2 \right), \\ \hat{d}_2 \tilde{d}_2 = -\frac{1}{2} \left(\tilde{d}_2^2 - {d_2}^2 + \hat{d}_2^2 \right). \end{cases} \tag{49}$$

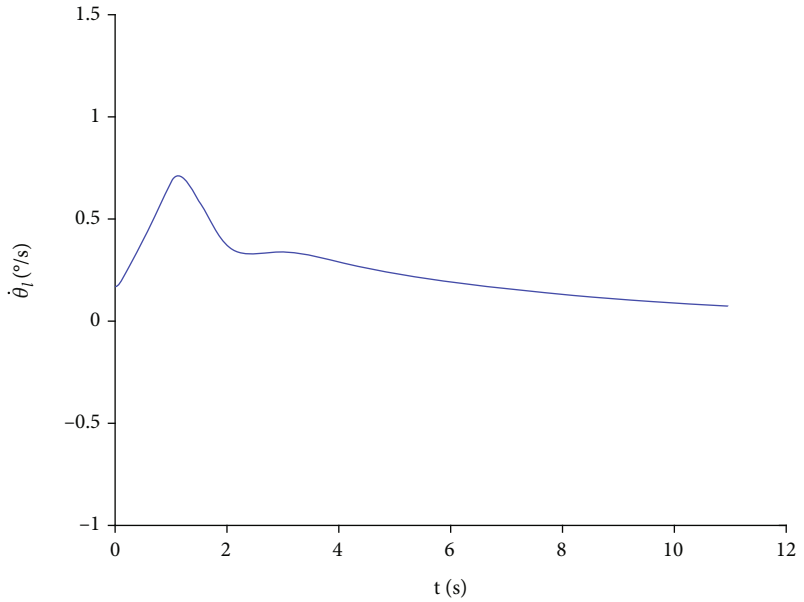

Figure 10: LOS angular rate curve.

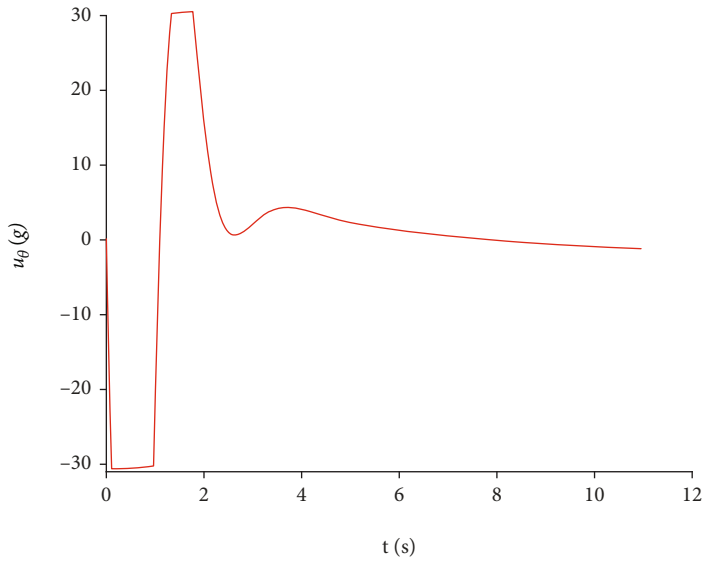

Figure 11: Missile acceleration curve.

We could obtain

$$\begin{aligned}\dot{V} &= \dot{V}_{\varepsilon 1} + \dot{V}_{z2} + \dot{V}_{z3} + \dot{V}_{2y} + \dot{V}_{3y} \\ &= -c_2 k_1 \varepsilon_1^2 - k_2 z_2^2 - k_3 z_3^2 - c_2 \frac{r_1}{\rho_1} \frac{1}{R} y_2 \varepsilon_1 + z_2 y_3 - \sigma_1 \frac{1}{2} \tilde{d}_1^2 \\ &\quad + \sigma_1 \frac{1}{2} {d_1}^2 - \sigma_1 \frac{1}{2} {\hat{d}_1}^2 - \sigma_2 \frac{1}{2} \tilde{d}_2^2 + \sigma_2 \frac{1}{2} {d_2}^2 - \sigma_2 \frac{1}{2} {\hat{d}_2}^2 \\ &\quad - \frac{2y_2^2}{\tau_2} + y_2 \eta_2 - \frac{2y_3^2}{\tau_3} + y_3 \eta_3,\end{aligned} \tag{50}$$

where $-\sigma_1(1/2){\hat{d}_1}^2 - \sigma_2(1/2){\hat{d}_2}^2 < 0$, so we could obtain

$$\begin{aligned}\dot{V} &\le -c_2 k_1 \varepsilon_1^2 - k_2 z_2^2 - k_3 z_3^2 - \sigma_1 \frac{1}{2} \tilde{d}_1^2 - \sigma_2 \frac{1}{2} \tilde{d}_2^2 - \frac{2y_3^2}{\tau_3} \\ &\quad + y_3 \eta_3 + \sigma_1 \frac{1}{2} {d_1}^2 + \sigma_2 \frac{1}{2} {d_2}^2 - c_2 \frac{r_1}{\rho_1} \frac{1}{R} y_2 \varepsilon_1 + z_2 y_3 \\ &\quad - \frac{2y_2^2}{\tau_2} + y_2 \eta_2,\end{aligned} \tag{51}$$

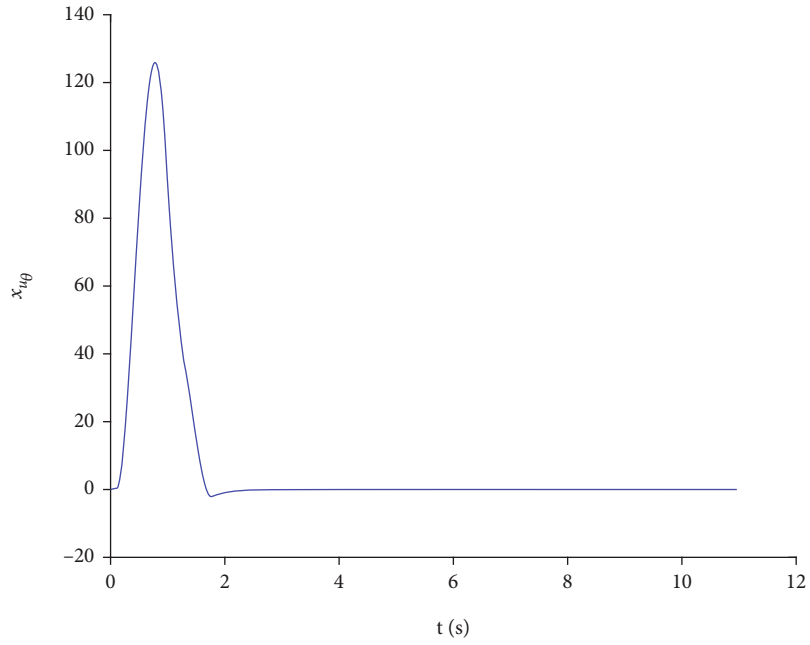

Figure 12: Variation curve of auxiliary variables.

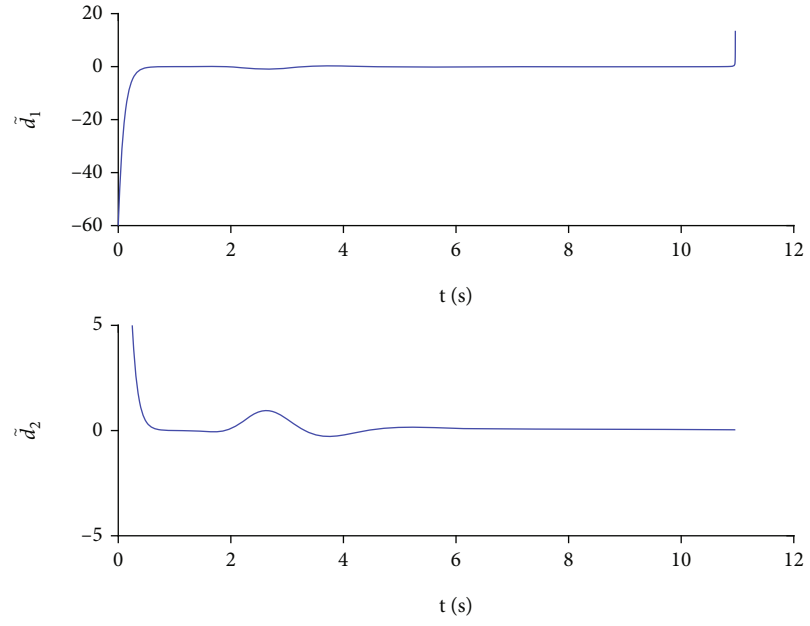

Figure 13: Estimation error curve.

where d_1 and d_2 are all bounded disturbances, so it is clear that $\sigma_1(1/2){d_1}^2$, $\sigma_2(1/2){d_2}^2$ are all bounded. Setting bounded interference upper bound to L_d

$$\sigma_1 \frac{1}{2} {d_1}^2 + \sigma_2 \frac{1}{2} {d_2}^2 \le L_d. \tag{52}$$

The scale of $\dot{V}$ can be further determined

$$\dot{V} \le -c_2 k_1 \varepsilon_1^2 - k_2 z_2^2 - k_3 z_3^2 - \sigma_1 \frac{1}{2} \tilde{d}_1^2 - \sigma_2 \frac{1}{2} \tilde{d}_2^2 - c_2 \frac{r_1}{\rho_1} \frac{1}{R} \varepsilon_1 y_2 + z_2 y_3 - \frac{2y_2^2}{\tau_2} + y_2 \eta_2 - \frac{2y_3^2}{\tau_3} + y_3 \eta_3 + L_d. \tag{53}$$

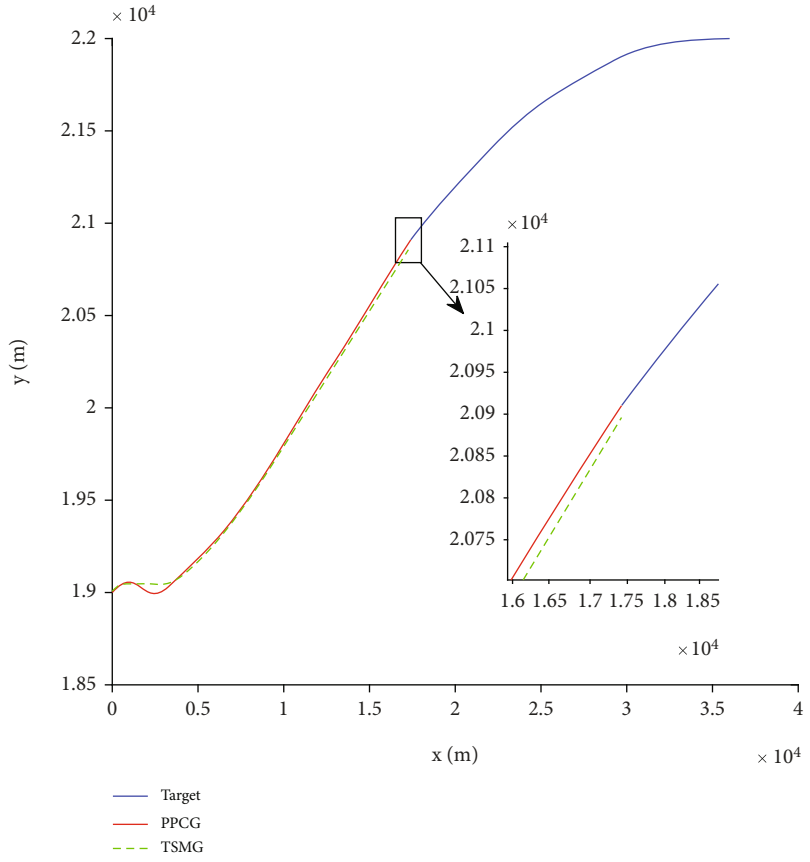

Figure 14: Trajectory curve.

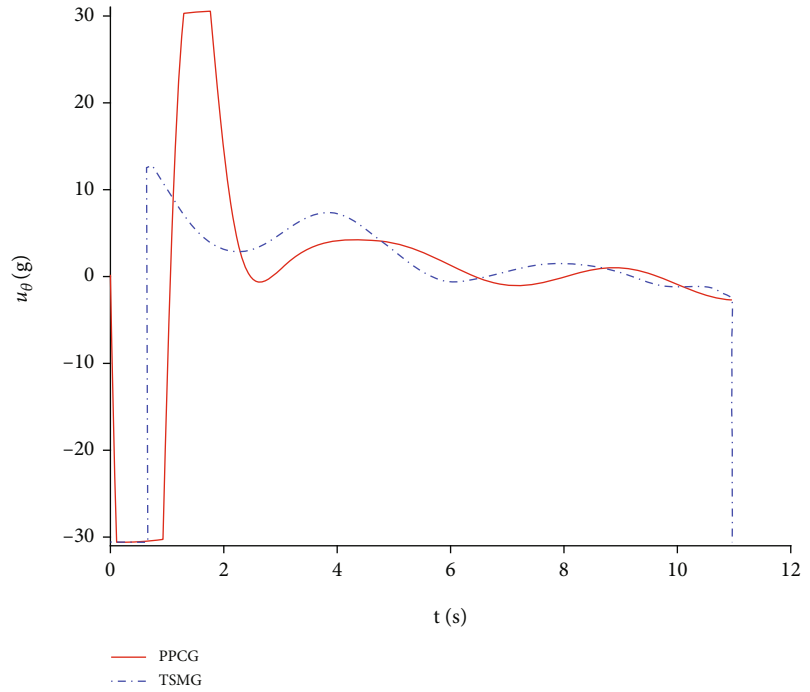

Figure 15: Comparison of missile acceleration curve.

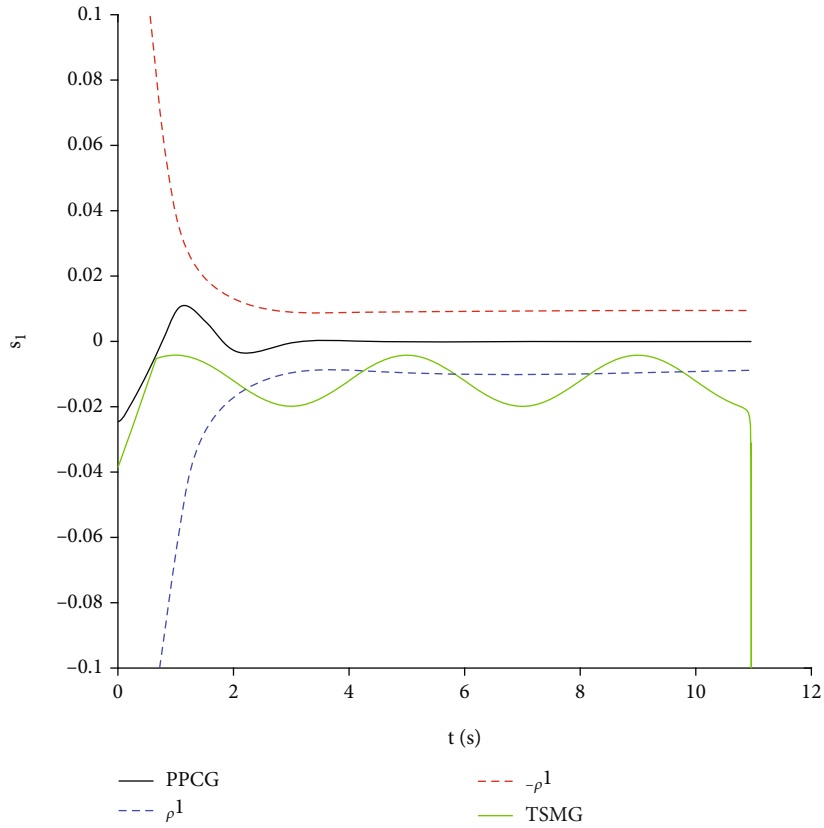

Figure 16: Comparison of slip surface changes.

On the basis of

$$-c_2\frac{r_1}{\rho_1}\frac{1}{R}\varepsilon_1 y_2 + z_2 y_3 + y_2\eta_2 + y_3\eta_3 \le \left|c_2\frac{r_1}{\rho_1}\frac{1}{R}\varepsilon_1 y_2\right| + |z_2 y_3| + |y_2\eta_2| + |y_3\eta_3|. \tag{54}$$

We could obtain

$$\dot{V} \le -c_2 k_1\varepsilon_1^2 - k_2 z_2^2 - k_3 z_3^2 - \sigma_1\frac{1}{2}\tilde{d}_1^2 - \sigma_2\frac{1}{2}\tilde{d}_2^2 - \frac{2y_2^2}{\tau_2} - \frac{2y_3^2}{\tau_3} + \left|c_2\frac{r_1}{\rho_1}\frac{1}{R}\varepsilon_1 y_2\right| + |z_2 y_3| + |y_2\eta_2| + |y_3\eta_3| + L_d. \tag{55}$$

In consideration of

$$\begin{aligned}\varepsilon_1 y_2 &\le \frac{1}{2}\varepsilon_1^2 + \frac{1}{2}y_2^2,\\ z_2 y_3 &\le \frac{1}{2}z_2^2 + \frac{1}{2}y_3^2,\\ y_i\eta_i &\le \frac{1}{2}y_i^2 + \frac{1}{2}\eta_i^2,\end{aligned} \tag{56}$$

we could obtain

$$\dot{V} \le -c_2\left(k_1 - \frac{1}{2}\frac{r_1}{\rho_1}\frac{1}{R}\right)\varepsilon_1^2 - \left(k_2 - \frac{1}{2}\right)z_2^2 - k_3 z_3^2 - \sigma_1\frac{1}{2}\tilde{d}_1^2 - \sigma_2\frac{1}{2}\tilde{d}_2^2 - \left(\frac{2}{\tau_2} - 1\right)y_2^2 - \left(\frac{2}{\tau_3} - 1\right)y_3^2 + \frac{1}{2}\eta_2^2 + \frac{1}{2}\eta_3^2 + L_d. \tag{57}$$

Setting $L_\eta = (1/2)\eta_2^2 + (1/2)\eta_3^2$ and substituting L_η into equation (57), we could obtain

$$\dot{V} \le -c_2\left(k_1 - \frac{1}{2}\frac{r_1}{\rho_1}\frac{1}{R}\right)\varepsilon_1^2 - \left(k_2 - \frac{1}{2}\right)z_2^2 - k_3 z_3^2 - \sigma_1\frac{1}{2}\tilde{d}_1^2 - \sigma_2\frac{1}{2}\tilde{d}_2^2 - \left(\frac{2}{\tau_2} - 1\right)y_2^2 - \left(\frac{2}{\tau_3} - 1\right)y_3^2 + L_\eta + L_d, \tag{58}$$

$$C_{\min} = \begin{pmatrix} -c_2\left(k_1 - \frac{1}{2}\frac{r_1}{\rho_1}\frac{1}{R}\right), -\left(k_2 - \frac{1}{2}\right) \\ -k_3, -\sigma_1\frac{1}{2}, -\sigma_2\frac{1}{2}, -\left(\frac{2}{\tau_2} - 1\right) \\ -\left(\frac{2}{\tau_3} - 1\right) \end{pmatrix}. \tag{59}$$

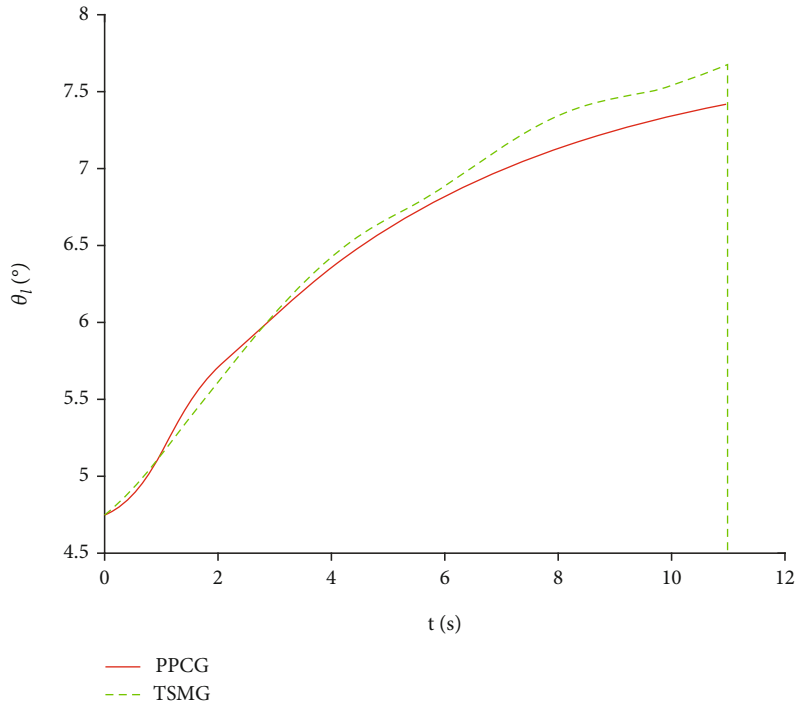

Figure 17: Comparison of LOS angular changes.

According to equation (59), equation (58) can be rewritten as

$$\dot{V} \le -C_{\min} V + L_\eta + L_d,$$
$$\Omega = \frac{L_\eta + L_d}{C_{\min}}. \tag{60}$$

Accordingly, as long as $C_{\min} \ge (L_\eta + L_d)/\Omega$, when $V \ge \Omega$, we have $\dot{V} \le 0$, so that $V \le \Omega$ is an invariant set. If $V(0) \le \Omega$, it is true for all $t > 0$ satisfies $V(t) \le \Omega$. Therefore, as long as appropriate parameters such as $k_1, k_2, k_3, \sigma_1, \sigma_2, \tau_2$, and τ_3 are selected, the LOS angle rate and LOS angle can converge to a sufficiently small error range.

The upper bound of the converge time can be defined as

$$t_r = \frac{1}{l_1} \ln\left(\frac{\rho_{0,1} - \rho_{\infty,1}}{\rho_r}\right), \tag{61}$$

where ρ_r is a smaller positive constant; we could obtain t_r from $\rho_1(t)$. Setting $\rho_1(t) \le \rho_{\infty,1} + \rho_r$, we could obtain

$$\begin{aligned} \left(\rho_{0,1} - \rho_{\infty,1}\right) \exp\left(-l_1 t\right) + \rho_{\infty,1} &\le \rho_{\infty,1} + \rho_r, \\ \left(\rho_{0,1} - \rho_{\infty,1}\right) \exp\left(-l_1 t\right) &\le \rho_r, \\ t &\ge \frac{1}{l_1} \ln\left(\frac{\rho_{0,1} - \rho_{\infty,1}}{\rho_r}\right). \end{aligned} \tag{62}$$

So, when $t \ge t_r$, the s_1 will eventually be limited to the following range:

$$-\iota_{\text{down},1}\left(\rho_{\infty,1} + \rho_r\right) < s_1 < \iota_{\text{up},1}\left(\rho_{\infty,1} + \rho_r\right). \tag{63}$$

□

6. Numerical Simulation

In order to verify the effectiveness of the prescribed performance guidance law (PPCG), first is verifying whether the PPCG can meet different terminal line of LOS angle constraint when the target is not maneuvering; secondly, the PPCG is simulated under two modes: arc maneuver and spiral maneuver in the circular; at the end, the simulation is compared PPCG with the fast terminal sliding mode guidance law (TSMG) under the same simulation conditions to highlight the characteristics of the PPCG.

Setting missile velocity $V_M = 1000$ m/s, initial trajectory inclination is 60°, and initial position coordinate is 0 m and 5000 m. The target velocity is $V_T = 700$ m/s, the blind area of the seeker is $r_b = 300$ m, the initial trajectory angle of the target is 0°, and the initial position coordinates is 15000 m and10000 m. The expected LOS angle is 45°, the simulation step is 0.001 s, and the interceptor acceleration is limited to ±15 g; ι_{up} and ι_{down} are converged in the following form:

$$\begin{cases} \dfrac{d}{dt}\iota_{\text{up}} = -2\iota_{\text{up}} + 1, \\ \dfrac{d}{dt}\iota_{\text{down}} = -2\iota_{\text{down}} + 1. \end{cases} \tag{64}$$

The guidance law parameters are selected as $\rho_{0,1} = 2$,

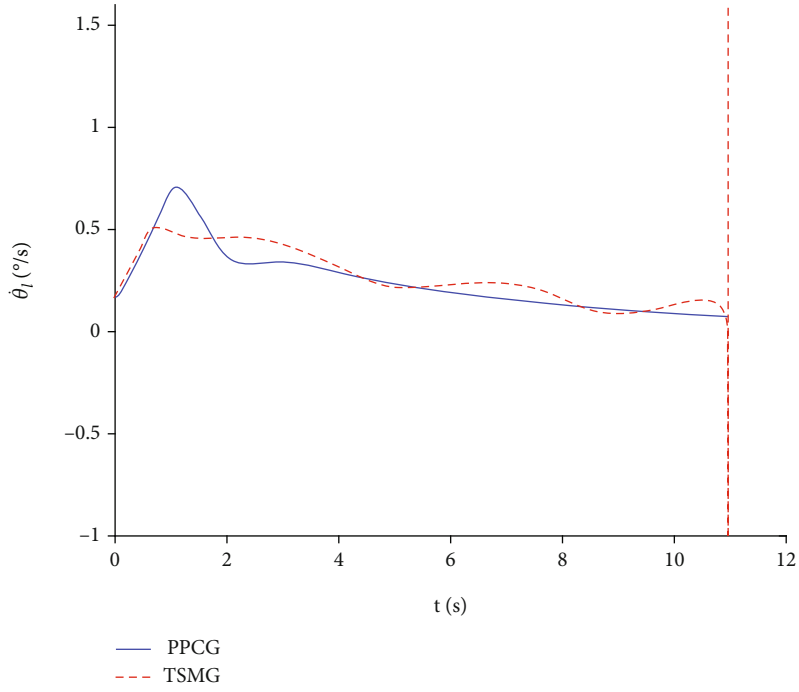

Figure 18: Comparison of LOS angular rate changes.

$\rho_{\infty,1} = 2$, $l_1 = 0.3$, $k_1 = 1.5$, $k_2 = 0.5$, $k_3 = 0.3$, and $k_{u_\theta} = 2.5$. The filtering parameter is selected as $\tau_1 = 0.01$ and $\tau_2 = 0.01$. The adaptive law parameter is selected as $\sigma_1 = 0.8$ and $\sigma_2 = 0.8$. The parameters of interceptor autopilot are selected as $\zeta = 0.8$, $\omega_n = 8$ rad/s, and $d_2 = 200 \sin(t)$.

Case 1. Tracking different expected LOS angle when target is not maneuvering. The simulation results are shown in Figures 2–6.

It can be seen from Figures 2 and 4 that the PPCG can satisfy different terminal LOS angle constraint, and the LOS angle gradually converges to the expected LOS angle as the interception proceeds. Figure 5 shows that the LOS angle rate converges rapidly to zero, and the interceptor is close to zero-control interception state. Correspondingly, in Figure 3, the acceleration of the interceptor has been saturated in the first 2 s of the simulation to adjust the direction of the interceptor speed. Figure 6 shows that the sliding mode variable can converge in preset range. In different LOS angle constraints, sliding mode variables have similar convergence performance under the same PPF, and the upper bound of the converge time is about 4.054 s.

Case 2. The target performs circular arc maneuver with $a_{Tly} = 2g$ in the longitudinal plane, the expected LOS angle is 7.8°, and the simulation results are shown in Figures 7–13.

According to the simulation results, the duration of the whole interception process is 10.94 s, and the final miss-distance is 0.018 m, indicating that the PPCG designed in this paper can meet the requirements of accurate attack on the constant maneuvering target. Figure 8 shows the variation curve of the sliding mode variable which can be seen that the sliding mode variable can converge in the prescribed performance range under the action of PPCG, and the convergence time is about 2.8 s. The sliding mode variable changes gently in the convergence process and can continue to maintain smooth and no chattering after convergence. From Figures 9 and 10, it can be seen that the convergence characteristics of the LOS angular rate are basically consistent with the sliding mode variable and the LOS angle finally reaching the expected angle. As shown in Figures 11 and 12, when the acceleration is close to saturation, the auxiliary system compensates the tracking error of the sliding mode variable. Even if the acceleration is in an instantaneous saturated state, the sliding mode variable can still be stabilized near zero. When the acceleration is in a saturated state, the state variable χ_{u_θ} of the auxiliary system can provide effective compensation for the tracking error of the sliding mode variable in time, so as to ensure the steady change of LOS angle and LOS angular rate.

It can be seen from Figure 13 that the estimation errors $\tilde{d}_1$ and $\tilde{d}_2$ can converge within 1.8 s. The uncertainty in PPCG is compensated by using the estimation information output by the adaptive law, and the target can be intercepted successfully when the target is maneuvering, and the uncertainty of autopilot is considered. Therefore, it has a good ability of uncertainty compensation.

Case 3. Target performs sinusoidal maneuvering with $a_{Tly} = 2g + g \sin(\pi t/4)$ in the longitudinal plane. In order to further highlight the superiority of the proposed PPCG, it is compared with TSMG for simulation. The specific form of TSMG is as follows:

$$s = x_2 + k_1 x_1 + k_2 \operatorname{sign}(x_1) |x_1|^\rho,$$

$$u_{SMG} = -2\dot{R}x_2 + R\gamma_1 \text{ sign } (s) + R\left(k_1 x_2 + k_2 \rho x_2 \text{ sign } (x_1)|x_1|^{\rho-1}\right) + R\left(\zeta_1 s + \zeta_2 |s|^{\delta} \text{ sign } (s)\right), \tag{65}$$

where

$$\begin{aligned} \zeta_1 &= 1.7, \\ \zeta_2 &= 1.5, \\ \delta &= \frac{3}{5}, \\ k_1 &= 1.8, \\ k_2 &= 1.9, \\ \rho &= \frac{3}{5}, \\ \gamma_1 &\geq \left|a_{Tly}\right|. \end{aligned} \tag{66}$$

The simulation conditions are the same as those in Case 2, and the simulation results are shown in Figures 14–18.

It can be seen from the simulation results that, on the whole, the interception time of the two guidance laws is similar; all of them can meet the requirements of maneuvering target interception, but the miss-distance of TSMG is larger than PPCG. Figure 16 shows that the sliding mode variable of TSMG and PPCG has good convergence characteristics. However, the transient performance and steady-state performance of TSMG are not as good as PPCG. The sliding mode variable of PPCG can converge according to the prescribed performance, and the convergence accuracy is higher than TSMG. In terms of convergence speed, PPCG is also faster than TSMG. TSMG cannot overcome the impact of target maneuver and autopilot delay and cannot adjust missile acceleration in time when it is saturated, which cause larger fluctuations in LOS angle and LOS angular rate compared to PPCG as shown in Figures 17 and 18. In contrast, the PPCG with auxiliary variables proposed in this paper is more conducive to missile execution.

7. Conclusions

This paper focuses on the guidance law design of interceptor hitting high-speed maneuvering targets under multiple constraints, and the main work is as follows:

First, in order to meet the actual interception process, a two-dimensional relative guidance model is established under the constraints of interceptor's terminal LOS angle, autopilot's second-order dynamic delay characteristic, and the saturation constraint of interceptor's acceleration. Then, based on the prescribed performance control theory and the dynamic surface control method, a prescribed performance control guidance law is designed under multiple constraints, and an auxiliary system is designed to compensate for the influence of limited input on the guidance system of interceptor missile, guaranteeing that the LOS angle and LOS angular rate can converge to the expected value in limited time according to the prescribed performance function. The stability of the guidance law is proved strictly by Lyapunov theorem, and its validity is verified by numerical simulation.

PPCG can overcome the influence of target maneuver, attenuate the effects of autopilot delay, and adjust acceleration saturation. Setting the parameters of PPCG is convenient, and the same set of parameters can adapt to different interception situations and satisfy multiple constraints. However, PPCG's ability to deal with constraints is limited, and the prescribed performance function adopted has problems of uncontrollable convergence time and overshoot. Therefore, how to design a prescribed performance function with controllable convergence time and overshoot to further improve the ability of PPCG to deal with constraints is worthy of further study.

Data Availability

The data sources from the references are all marked in this paper. And the parameters designed are all described in this paper. Therefore, the data in this paper has been fully covered and can be obtained.

Conflicts of Interest

The authors declare that they have no conflicts of interest.

Acknowledgments

The authors would like to thank the Air and Missile Defense college of Air Force Engineering University of China for helpful discussions on topics related to this work. This study was cosupported by the National Natural Science Foundation of China (Grant nos. 62173339 and 61873278).

References

[1] D. Zhou, P. Qu, and S. Sun, "A guidance law with terminal impact angle constraint accounting for missile autopilot," *Journal of Dynamic Systems, Measurement, and Control*, vol. 135, no. 5, article 051009, 2013.

[2] S. He, D. Lin, and J. Wang, "Robust terminal angle constraint guidance law with autopilot lag for intercepting maneuvering targets," *Nonlinear Dynamics*, vol. 81, no. 1-2, pp. 881–892, 2015.

[3] G. Hexner, T. Shima, and H. Weiss, "LQC guidance law with bounded acceleration command," *IEEE Transactions on Aerospace and Electronic Systems*, vol. 44, no. 1, pp. 77–86, 2008.

[4] C. Lee, T. Kim, M. Tahk, and I. H. Whang, "Polynomial guidance laws considering terminal impact angle and acceleration constraints," *IEEE Transactions on Aerospace and Electronic Systems*, vol. 49, no. 1, pp. 74–92, 2013.

[5] C. Shieh, "Design of three-dimensional missile guidance law via tunable nonlinear Hoo control with saturation constraint," *IET Control Theory and Applications*, vol. 1, no. 3, pp. 756–763, 2007.

[6] Z. Wenjie, F. U. Shengnan, L. I. Wei, and X. I. Qunli, "An impact angle constraint integral sliding mode guidance law for maneuvering targets interception," *Journal of Systems Engineering and Electronics*, vol. 31, no. 1, pp. 168–184, 2020.

[7] W. J. Zhang, Q. L. Xia, and W. Li, "Novel second-order sliding mode guidance law with an impact angle constraint that considers autopilot lag for intercepting manoeuvering targets," *The Aeronautical Journal*, vol. 124, no. 1279, pp. 1350–1370, 2020.

[8] C. Zhang, K. Zhang, and J. Wang, "An adaptive terminal sliding mode guidance law for head pursuit interception with impact angle considered," in *Informatics in Control Automation and Robotics*, pp. 277–292, Springer, Cham, 2018.

[9] Z. Zhao, J. Yang, S. Li, and C. Man, "Continuous terminal sliding mode guidance law with consideration of autopilot dynamics," in *IECON 2017-43rd Annual Conference of the IEEE Industrial Electronics Society*, Beijing, China, 2017.

[10] J. Yang, J. Yan, and J.-L. Wei, "Research on adaptive sliding mode guidance law based on parallel approach," *Aeronautical Computing Technique*, vol. 3, 2018.

[11] S. Zhai, X. Wei, and J. Yang, "Cooperative guidance law based on time-varying terminal sliding mode for maneuvering target with unknown uncertainty in simultaneous attack," *Journal of the Franklin Institute*, vol. 357, no. 16, pp. 11914–11938, 2020.

[12] S. R. Kumar, S. Rao, and D. Ghose, "Nonsingular terminal sliding mode guidance with impact angle constraints," *Journal of Guidance, Control, and Dynamics*, vol. 37, no. 4, pp. 1114–1130, 2014.

[13] Z. Zhang, S. Li, and S. Luo, "Composite guidance laws based on sliding mode control with impact angle constraint and autopilot lag," *Transactions of the Institute of Measurement and Control*, vol. 35, no. 6, pp. 764–776, 2013.

[14] D. Zhou and X. Biao, "Adaptive dynamic surface guidance law with input saturation constraint and autopilot dynamics," *Journal of Guidance, Control, and Dynamics*, vol. 39, no. 5, pp. 1155–1162, 2016.

[15] S. He and D. Lin, "Observer-based guidance law against maneuvering targets without line-of-sight angular rate information," *Proceedings of the Institution of Mechanical Engineers, Part G: Journal of Aerospace Engineering*, vol. 230, no. 10, pp. 1827–1839, 2016.

[16] H. Zhou, S. Song, J. Song, and J. Niu, "Design of second-order sliding mode guidance law based on the nonhomogeneous disturbance observer," *Journal of Control Science and Engineering*, vol. 2014, 10 pages, 2014.

[17] Y. Sheng, Z. Zhang, and L. Xia, "Fractional-order sliding mode control based guidance law with impact angle constraint," *Nonlinear Dynamics*, vol. 106, no. 1, pp. 425–444, 2021.

[18] S. Chakrabarty and B. Bandyopadhyay, "A generalized reaching law for discrete time sliding mode control," *Automatica*, vol. 52, pp. 83–86, 2015.

[19] X. Bu and Q. Qi, "Fuzzy optimal tracking control of hypersonic flight vehicles via single-network adaptive critic design," *IEEE Transactions on Fuzzy Systems*, vol. 30, no. 1, pp. 270–278, 2022.

[20] X. Bu, Q. Qi, and B. Jiang, "A simplified finite-time fuzzy neural controller with prescribed performance applied to waverider aircraft," *IEEE Transactions on Fuzzy Systems*, vol. 1, p. 1, 2021.

[21] X. Bu, "Air-breathing hypersonic vehicles funnel control using neural approximation of non-affine dynamics," *IEEE/ASME Transactions on Mechatronics*, vol. 23, no. 5, pp. 2099–2108, 2018.

[22] Q. Hu, X. Shao, and L. Guo, "Adaptive fault-tolerant attitude tracking control of spacecraft with prescribed performance," *IEEE/ASME Transactions on Mechatronics*, vol. 23, no. 1, pp. 331–341, 2018.

[23] Y. Shi, X. Shao, and W. Zhang, "Quantized learning control for flexible air-breathing hypersonic vehicle with limited actuator bandwidth and prescribed performance," *Aerospace Science and Technology*, vol. 97, article 105629, 2020.

[24] P. P. Qu and D. Zhou, "Guidance law incorporating secondorder dynamics of missile autopilots," *Systems Engineering and Electronics*, vol. 33, no. 10, pp. 2263–2267, 2011.